

Introduction

In areas of high structural complexity (e.g., near salt bodies), borehole seismic data may give detailed subsurface information that cannot be obtained from surface seismic data. Seismic interferometry (Curtis et al., 2006) opens possibilities for innovative uses of borehole seismic data, because seismic interferometry reconstructs waves that propagate between receivers as if one of them acted as a source. Hence, with interferometry, it is possible to “create” pseudo-acquisition geometries that differ from the original physical experiments. Schuster et al. (2004) used the concept of interferometry to migrate free-surface reflections from Reverse VSP data. The Virtual Source method of Bakulin and Calvert (2006) is used to image beneath a complex overburden from borehole sensors placed in a horizontal well with no knowledge of the overburden model parameters. In the context of salt flank imaging, Willis et al. (2006) presented a numerical example demonstrating that diving waves can be used for the interferometric imaging of near-vertical salt reflectors.

Although no knowledge of model parameters is necessary for the interferometry of internal multiples, this method relies on wavefield separation to select waves propagating in specific directions between receivers (Vasconcelos and Snieder, 2008a; Vasconcelos, 2008). For this reason, we refer to this method as *target-oriented* interferometry. Apart from being suitable to image features above the receiver array, target-oriented interferometry can also be tailored to image below the array. In that case, our method is analogous to the Virtual Source applications of Bakulin and Calvert (2006) and Mehta et al. (2007).

Target-oriented interferometry

A form of interferometry that targets the extraction of the wavefield perturbation $G_S(\mathbf{r}_A, \mathbf{r}_B, \omega)$, measured at \mathbf{r}_A and excited by a pseudo-source at \mathbf{r}_B is (Vasconcelos, 2008; Vasconcelos and Snieder, 2008a)

$$\int_{\sigma_i} u_S(\mathbf{r}_A, \mathbf{s}) u_0^*(\mathbf{r}_B, \mathbf{s}) d\mathbf{s} \approx \langle |W(\mathbf{s})|^2 \rangle G_S(\mathbf{r}_A, \mathbf{r}_B); \quad (1)$$

where the integration over sources is no longer conducted over the closed surface Σ , but rather over a part of it, denoted by σ_i (e.g., σ_1 or σ_2 in Figure 1). u_0 and u_S are the recorded reference and scattered fields; respectively. Below we describe a method that selects waves in u_0 by wavefield separation.

To perform target-oriented interferometry according to equation 1, we select specific arrivals in u_0 and u_S (Figure 1) with a two-step procedure. First, we choose the segment σ_i based on the relative position of the receivers and the portion of the surface we wish to image (volume \mathbb{P}). For example, the sources over σ_1 excites direct waves that propagate downward and rightward in Figure 1a, that once reflected in the unperturbed medium are recorded as the up-going waves u_0 that are illustrated in the figure. In the case of Figure 1b, the sources over σ_2 are the ones that radiate energy directly down towards the receivers, being thus suitable for reconstructing the desired scattered perturbations from interferometry (Vasconcelos, 2008; Bakulin and Calvert, 2006; Mehta et al., 2007).

In a second step, we separate u_0 and u_S from u according to the direction of the incoming waves at a given receiver. The direction of incoming waves, in the time-domain, can be inferred from the slopes of the arrivals in the recorded shot gathers (i.e., for a fixed source and multiple receivers). These slopes translate to the apparent shot-domain wavenumbers, which we refer to as k_s . Figure 2a describes the wavefield separation necessary to target the imaging of scatterers above the receiver array, as in Figure 1a. In this case, keeping the negative shot-domain wavenumbers at \mathbf{r}_B (left-hand side of Figure 2a) defines $u_0(\mathbf{r}_B, \mathbf{s}, \omega)$ (equation 1), which contains mostly up-going incoming waves. This ensures that the pseudo-source at \mathbf{r}_B (see equation 1) radiates mostly up-going energy. For the receivers that record the interferometric data, represented by \mathbf{r}_A , the choice of incoming wave direction depends on the relative positioning between a given receiver and the pseudo-source at \mathbf{r}_B . If the receiver is above the pseudo-source

(top cartoon on right-hand side of Figure 2a), waves with $k_s < 0$ give $u_S(\mathbf{r}_A, \mathbf{s}, \omega)$ (see equation 1). For \mathbf{r}_A below \mathbf{r}_B , we use waves with $k_s > 0$ to extract $u_S(\mathbf{r}_A, \mathbf{s}, \omega)$. After wavefield separation as in Figure 2b, using $u_S(\mathbf{r}_A, \mathbf{s}, \omega)$ and $u_0(\mathbf{r}_B, \mathbf{s}, \omega)$ for different \mathbf{r}_A positions results in a pseudo-shot gather that radiates energy down toward the perturbation volume \mathbb{P} (Figure 1b). As mentioned above, the case of Figure 1b is also the objective of the Virtual Source method (Bakulin and Calvert, 2006; Mehta et al., 2007a).

Interferometry by deconvolution (Vasconcelos and Snieder, 2007) is an option for reconstructing an interferometric impulse response when estimates of the source power spectra are not available. When estimates of the power spectra of the source function are available, these can be used to extract the impulse response from interferometry (Wapenaar and Fokkema, 2006; Mehta et al., 2007). In particular, deconvolution interferometry can be more effective than its correlation-based counterpart in reconstructing impulsive pseudo-sources when the input excitation consists of a complicated, unknown waveform (Vasconcelos and Snieder, 2008b). This can be the case when using internal multiples to do interferometry.

Imaging multiples from subsalt VSP data

The purpose of this numerical example is to use the subsalt WAW VSP data to image the Sigsbee salt canopy from below by using the interference of internal multiples, analogous to the example in Figure 1. The experiment simulates the recording of shots placed 500 ft deep, at 100 evenly-spaced receivers in a deviated borehole (red lines in Figures 3 and 4). The first receiver is placed at $x = 48000$ ft and at a depth of 16000 ft; while the lateral and depth coordinates of the last receiver are 52950 ft and 20950 ft, respectively. The shots start at $x = 10000$ ft with a shot interval of 125 ft. The source waveform consists of a Ricker wavelet with 12 Hz peak frequency. In our experiments, we consider shots placed from $x = 10000$ ft to $x = 53500$ ft (this corresponds to the surface σ_1 in Figure 1a).

Interferometric images using the full recorded data (with no wavefield separation) are shown in Figure 3. The imaging in these examples is done by wavefield extrapolation in a slant coordinate system that conforms with the receiver array. Figure 3a is generated using cross-correlation interferometry while Figure 3b is obtained from deconvolution interferometry (Vasconcelos and Snieder, 2008b). The source function is suppressed by deconvolution interferometry (Figure 3b; Vasconcelos and Snieder, 2008b). The images in Figure 3 show an accurate reconstruction of the salt canopy, especially towards the right-hand side of the model where the salt flanks are dipping. Above the receiver array, the imaged salt is characterized by reflectors that are weak compared to the dipping salt flanks. The images of the sediments between the salt the receiver array are distorted and do not reproduce the horizontal bedding of the model (Figure 3).

After applying the target-oriented interferometry method based on wavefield separation illustrated by Figure 2a, we obtain the images in Figure 4. Note that although the original source and receiver geometry is the same for the images in Figures 3 and 4 is the same, the portion of the model illuminated by these two sets of images is substantially different. As discussed in the previous Section, the pseudo-sources reconstructed by target-oriented interferometry are designed to radiate energy upward (Figures 1a and 2a). Hence, the images in Figure 4 illuminate the model predominantly in the area above the receiver array. These images show bright reflectors at the bottom and top salt above the array, which appear as dim reflectors in the images in Figure 3. Figure 4b shows that the target-oriented interferometric images recover the structure of the subsalt sediments which are not seen in Figure 3. The reflector that corresponds to the dipping top salt (right-hand side of images in Figure 3) is not present in the images in Figure 4. This reflector is absent in the target oriented interferometric images because it is imaged in Figure 3 from reflections reconstructed from diving waves that arrive at the receiver array with positive shot-domain wavenumbers. Since the wavefield separation builds the filter u_0 from $k_s < 0$, reflectors from such diving waves are not present in Figure 4.

Conclusion

We present an interferometry technique based on wavefield separation in the shot-domain that targets the reconstruction of specific arrivals in the interferometric shot gathers. In particular, we promote that this target-oriented interferometry technique can be used to reconstruct single-reflected waves from internal multiples. The application of the technique consists in manipulating the recorded data to separate unperturbed waves at the receiver that acts as a pseudo-source, and wavefield perturbations at the receivers that record the interferometric experiment. We separate these wavefields according to the directions of the waves incoming at a given receiver; i.e., according to the shot-domain wavenumber.

Using the *Sigsbee* salt model, we illustrate how interferometric illumination can be controlled using wavefield separation along with the appropriate choice of sources to be included. The numerical experiment consists of a large-offset walkaway VSP recorded at a deviated 100-receiver array placed below the salt. Seismic interferometry with no wavefield separation yields an image of the salt body which is well defined in the dipping salt flanks to the right-hand side of the array. These reflectors are mainly sampled by diving waves, analogously to the numerical experiment by Willis et al. (2006). The images obtained from target-oriented interferometry recover the reflectors at the top and base of salt located immediately above the receiver array. These images also recover a portion the subsalt sediment structure that cannot be retrieved by the interferometry of the full recorded wavefields. In the *Sigsbee* example, the target-oriented interferometry procedure reconstructs down-going single-scattered waves from up-going internal multiples recorded in the original experiment. The results we present here can in principle be extended to perform elastic imaging of internal multiples using perturbation-based elastic interferometry (e.g., Gaiser and Vasconcelos, 2008).

References

- [1] A. Bakulin and R. Calvert. The virtual source method: Theory and case study. *Geophysics*, 71:SI139–SI150, 2006.
- [2] J. Gaiser and I. Vasconcelos. Elastic interferometry of OBC data – Theory and Examples. *EAGE Expanded Abstracts*, submitted, 2008.
- [3] K. Mehta, A. Bakulin, J. Sheiman, R. Calvert, and R. Snieder. Improving virtual source method by wave-field separation. *Geophysics*, 72:V79–V86, 2007.
- [4] G.T. Schuster, F. Followill, L.J. Katz, J. Yu, and Z. Liu. Autocorrelogram migration: Theory. *Geophysics*, 68:1685–1694, 2004.
- [5] I. Vasconcelos and R. Snieder. Representation theorems and Green’s function retrieval in perturbed acoustic media. *Phys. Rev. E*, submitted, 2008a.
- [6] I. Vasconcelos and R. Snieder. Interferometry by deconvolution – Theory for acoustic waves and numerical examples. *Geophysics*, accepted, 2008b.
- [7] I. Vasconcelos. Perturbation-based interferometry – Applications and connection to seismic imaging. *EAGE Expanded Abstracts*, submitted, 2008.
- [8] K. Wapenaar and J. Fokkema. Green’s function representations for seismic interferometry. *Geophysics*, 71:SI133–SI146, 2006.
- [9] M.E. Willis, R. Lu, X. Campman, M.N. Toksöz, Y. Zhang, and M.V. de Hoop. A novel application of time-reversed acoustics: Salt-dome flank imaging using walkaway VSP surveys. *Geophysics*, 71:A7–A11, 2006.

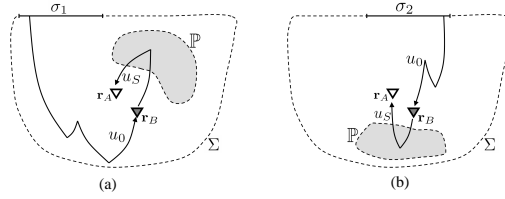


Figure 1: Illustrations of the perturbation approach to target-oriented interferometric imaging. The volume is bounded by Σ and contains medium perturbations in the volume \mathbb{P} (indicated by the grey-shaded areas). In both panels, u_0 are unperturbed wavefields, while u_S are wavefield perturbations due to scattering within the volume \mathbb{P} . The solid lines illustrate stationary wave-paths. Two receivers, located at \mathbf{r}_A and \mathbf{r}_B , are represented by the triangles. The grey triangle denotes the receiver that acts as a pseudo-source in the interferometric experiments.

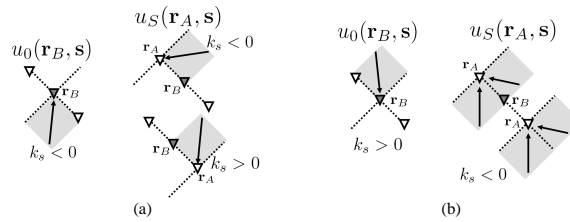


Figure 2: Panel (a) illustrates the separation of wavefields necessary for target-oriented interferometric imaging in the context of Figure 1a. The wavefield separation in panel (b) is designed for the imaging experiment in Figure 1b. The arrows indicate the direction of waves arriving at the receivers. k_s is the recorded-wave shot-domain wavenumber.

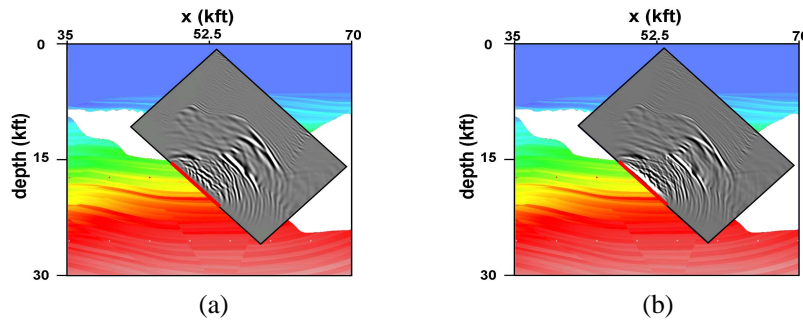


Figure 3: Images obtained from full-wavefield interferometry. The images, in grey scale, are superposed on the *Sigsbee* velocity model. The images are based on cross-correlation interferometry (panel a), and on deconvolution interferometry (panel b).

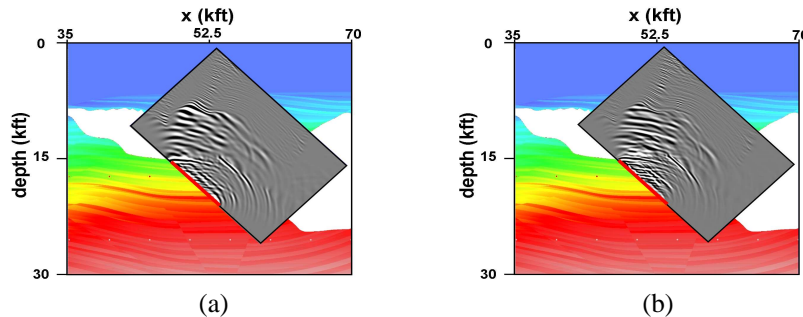


Figure 4: Images obtained from target-oriented interferometry of the *Sigsbee* walkaway VSP data. As in Figure 3, the image in (a) is obtained from cross-correlation interferometry and the image in (b) from deconvolution interferometry.